ASME 2012 5th Annual Dynamic Systems and Control Conference joint with the JSME 2012 11th Motion and Vibration Conference
DSCC2012-MOVIC2012
October 17-19, 2012, Fort Lauderdale, Florida, USA

DSCC2012-MOVIC2012-8871

A NONLINEAR MODELING FRAMEWORK FOR AUTONOMOUS CRUISE CONTROL

Gábor Orosz
Department of Mechanical Engineering
University of Michigan
Ann Arbor, Michigan 48109
Email: orosz@umich.edu

Shrenik P. Shah
Department of Mechanical Engineering
University of Michigan
Ann Arbor, Michigan 48109
Email: shrek@umich.edu

ABSTRACT

A nonlinear modeling framework is presented for autonomous cruise control (ACC) equipped vehicles which allows one to analyze car-following scenarios in a wide range of velocities and headways. By designing the range policy as well as the controller one can improve the ride qualities for individual vehicles and increase the throughput of the overall traffic systems.

INTRODUCTION

Vehicular traffic has been studied for many decades and many different control methods has been developed (traffic lights, variable message signs) to regulate transportation systems; see [1] for a review. While traditional traffic control increases the efficiency, further improvement are possible by exploiting advanced vehicle technologies. In particular, one may use autonomous cruise control (ACC) devices to regulate the flow [2].

We propose a modeling framework for ACC equipped vehicles that allows one to implement nonlinear range policies that can be used for the entire velocity and headway range. Such vehicles are able to operate in stop-and-go conditions. To achieve this one needs to take into account nonlinearities in the system (like air drag). On the other hand, we also exploit nonlinearities when designing and implementing the range policy, so that it provides a smooth ride and also increases the road capacity. We propose a particular nonlinear range policy which is easy to handle analytically. We show that both plant and string stability can be ensured by appropriate choice of control gains. Such controller can be implemented in vehicles independent of the powertrain specifications (internal combustion engine, hybrid-electric vehicles, electric vehicles, etc.) and allows optimization in the entire torque and engine speed range (e.g., for energy consumption).

NONLINEAR ACC MODEL

We consider vehicles on a single lane as represented in the top panel of Fig. 1 where the positions x_n, the velocities v_n and the headways h_n are shown together with the vehicle length ℓ. We focus our attention on two consecutive vehicles and for simplicity we drop the indexes for the follower and use the subscript L for the leader. To model the longitudinal dynamics of the follower we assume no slip condition on the wheels and neglect the flexibility of the tires and the suspension. Applying the power law we obtain the differential equation for the velocity v

$$m_{\rm eff}\dot{v} = -mg\sin\phi - \gamma mg\cos\phi - k(v+v_{\rm w})^2 + \frac{\eta}{R}T_{\rm en}\,. \qquad (1)$$

The effective mass $m_{\rm eff} = m + J/R^2$ contains the mass of the vehicle m, the moment of inertia J of the rotating elements, and the wheel radius R. Furthermore, g is the gravitational constant, ϕ is the inclination angle, γ is the rolling resistance coefficient, k is the air drag constant, $v_{\rm w}$ is the velocity of the headwind, η is the gear ratio, and $T_{\rm en}$ is the engine torque [3]. For simplicity, we consider $\phi = 0$, $v_{\rm w} = 0$ and $J = 0 \Longrightarrow m_{\rm eff} = m$, while the other parameters are shown in Table 1 in the Appendix. When units are not spelled out, quantities should be understood in SI units.

Our goal is to implement a given range policy $v = V(h)$ which is achieved by the vehicle in steady state. While a variety of range policies can be considered we assume the following general properties: (i) V is continuous and monotonously increasing (the more sparse traffic is, the faster the driver wants to travel); (ii) $V(h) \equiv 0$ for $h \leq h_{\rm st}$ (in dense traffic, drivers intend to stop); (iii) $V(h) \equiv v_{\rm max}$ for $h \geq h_{\rm go}$ (in very sparse traffic, drivers intend to drive with maximum speed – often called free flow speed). Indeed, vehicles that implement such range policy are capable of handling stop-and-go situations. Two examples are shown in the

Copyright © 2012 by ASME

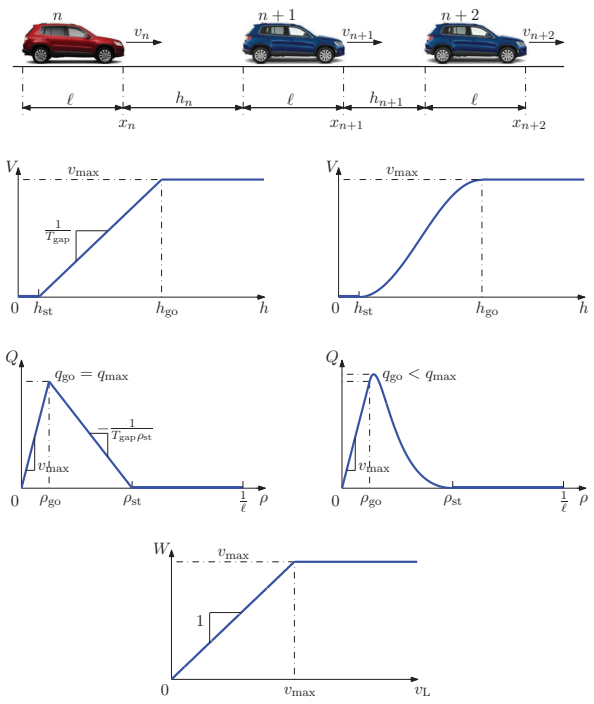

Figure 1. TOP ROW: SEQUENCE OF CARS ON A SINGLE LANE SHOWING VEHICLES' POSITIONS, VELOCITIES, AND HEADWAYS. SECOND ROW: TWO POSSIBLE RANGE POLICIES GIVEN BY (2) AND (3). THIRD ROW: THE CORRESPONDING FLUX DENSITY RELATIONSHIPS. BOTTOM ROW: THE SATURATION FUNCTION (5).

second row of Fig. 1. The nonsmooth function on the left represent a scenario where the time gap $T_{\text{gap}} = v_{\max}/(h_{\text{go}} - h_{\text{st}})$ is kept constant in the dynamic domain $h \in [h_{\text{st}}, h_{\text{go}}]$, that is,

$$V(h) = \begin{cases} 0 & \text{if} \quad h < h_{\text{st}}\,, \\ v_{\max}\frac{h-h_{\text{st}}}{h_{\text{go}}-h_{\text{st}}} & \text{if} \quad h_{\text{st}} \le h \le h_{\text{go}}\,, \\ v_{\max} & \text{if} \quad h > h_{\text{go}}\,, \end{cases} \tag{2}$$

while the smooth function on the right is given by

$$V(h) = \begin{cases} 0 & \text{if} \quad h < h_{\text{st}}\,, \\ \frac{v_{\max}}{2}\left(1 - \cos\left(\pi\frac{h-h_{\text{st}}}{h_{\text{go}}-h_{\text{st}}}\right)\right) & \text{if} \quad h_{\text{st}} \le h \le h_{\text{go}}\,, \\ v_{\max} & \text{if} \quad h > h_{\text{go}}\,. \end{cases} \tag{3}$$

Indeed, many other range policies are possible [1] and some models contain range policies implicitly [4]. The smooth function (3) provides smoother ride than (2) and also increases the overall throughput of the system as shown by the flux-density diagrams in the third row in Fig. 1. Here, the density and the flux are defined as $\rho = 1/(h+\ell)$ and $Q = \rho v = \rho V(1/\rho - \ell)$. (Such definition is only adequate in equilibrium situations where equidistant vehicles travel with constant velocity.) As can be observed the maximum flux is larger on the right. For the parameters shown in Table 1 in the Appendix, the maximum flux increases from 0.75 veh/s = 2700 veh/h to appr. 0.8 veh/s = 2880 veh/h which is considered significant in transportation systems. Indeed, the price one pays for the increase in flux is that in the middle of the dynamic domain the effective time gap becomes smaller. This must be compensated for by using appropriate control design.

To achieve a range policy as an equilibrium of the system we propose the controller

$$\begin{aligned} T_{\text{en}} &= K_{\text{p}}\dot{z} + K_{\text{i}} z + K_{\text{v}}\big(W(v_{\text{L}}) - v\big)\,, \\ \dot{z} &= V(h) - v\,, \end{aligned} \tag{4}$$

where the z variable is introduced to represent the integral of the error while the function

$$W(v_{\text{L}}) = \begin{cases} v_{\text{L}} & \text{if} \quad v_{\text{L}} \le v_{\max}\,, \\ v_{\max} & \text{if} \quad v_{\text{L}} > v_{\max}\,, \end{cases} \tag{5}$$

is introduced to avoid following the leader when its velocity is larger than $v_{\max}$; see the bottom panel in Fig. 1. In fact, the controller is similar to a sliding-mode controller with sliding surface $V(h) - v = 0$; see [5].

Using the plant model (1) and the controller (4) the closed-loop system can be written as

$$\begin{aligned} \dot{h} &= v_{\text{L}} - v\,, \\ \dot{v} &= -\gamma g - \frac{k}{m}v^2 + \hat{K}_{\text{p}}\dot{z} + \hat{K}_{\text{i}} z + \hat{K}_{\text{v}}\big(W(v_{\text{L}}) - v\big)\,, \\ \dot{z} &= V(h) - v\,, \end{aligned} \tag{6}$$

where

$$\hat{K}_{\text{p}} = \frac{K_{\text{p}}\eta}{mR}\,, \quad \hat{K}_{\text{i}} = \frac{K_{\text{i}}\eta}{mR}\,, \quad \hat{K}_{\text{v}} = \frac{K_{\text{v}}\eta}{mR}\,. \tag{7}$$

Note that $\hat{K}_{\text{p}}$ and $\hat{K}_{\text{v}}$ are measured in 1/s, $\hat{K}_{\text{i}}$ is measured in $1/\text{s}^2$, and $\hat{K}_{\text{p}}/\hat{K}_{\text{i}}$ represents the characteristic time needed to make the steady state error zero. For $v_{\text{L}} \le v_{\max}$ (ACC mode) this system possesses the equilibrium

$$v^* = v_{\text{L}}^*\,, \quad v^* = V(h^*)\,, \quad z^* = \frac{1}{\hat{K}_{\text{i}}}\left(\gamma g + \frac{k}{m}(v^*)^2\right), \tag{8}$$

where the last equation determines the engine torque $T_{\text{en}}^* = K_{\text{i}} z^* = \frac{mR}{\eta}\left(\gamma g + \frac{k}{m}(v^*)^2\right)$ required to maintain the equilibrium. For $v_{\text{L}} > v_{\max}$ (cruise control mode) the state $v^* = v_{\max}$ can be achieved though this not an equilibrium of (6). In this case, the follower simply operates in standard cruise control mode while the leader is getting away. It can be shown that this state is always stable.

Copyright © 2012 by ASME

PLANT STABILITY AND STRING STABILITY

In ACC mode ($v_{\rm L} \le v_{\rm max}$) one must ensure the stability of the system. By plant stability we simply mean that when the leader is driving with constant velocity then perturbations in the follower's states decay until the system reaches the equilibrium (8). On the other hand, string stability means that when the leader varies its velocity around a constant value, the fluctuations become smaller for the follower. In this section we will test these conditions by linearizing around the equilibrium. Indeed, this analysis only ensures linear plant and string stability, that valid for small perturbations.

Defining the perturbations $\tilde{h}(t) = h(t) - h^*$, $\tilde{v} = v(t) - v^*$, $\tilde{z}(t) = z(t) - z^*$ and $\tilde{v}_{\rm L}(t) = v_{\rm L}(t) - v_{\rm L}^*$ one may obtain the system

$$\frac{\rm d}{{\rm d}t}\begin{bmatrix}\tilde{h}\\ \tilde{v}\\ \tilde{z}\end{bmatrix} = \begin{bmatrix}0 & -1 & 0\\ \hat{K}_{\rm p}N_* & -\left(2\frac{k}{m}v^* + \hat{K}_{\rm p} + \hat{K}_{\rm v}\right) & \hat{K}_{\rm i}\\ N_* & -1 & 0\end{bmatrix}\begin{bmatrix}\tilde{h}\\ \tilde{v}\\ \tilde{z}\end{bmatrix} + \begin{bmatrix}1\\ \hat{K}_{\rm v}\\ 0\end{bmatrix}\tilde{v}_{\rm L} \quad (9)$$

where the symbol N_* represents the derivative of the range policy. For (3) this can be expressed as

$$N_* = V'(h^*) = \begin{cases} 0 & \text{if} \quad h < h_{\rm st}\,,\\ \frac{\pi}{2}\frac{v_{\rm max}}{h_{\rm go}-h_{\rm st}}\sin\left(\pi\frac{h^*-h_{\rm st}}{h_{\rm go}-h_{\rm st}}\right) & \text{if} \quad h_{\rm st} \le h \le h_{\rm go}\,,\\ 0 & \text{if} \quad h > h_{\rm go}\,,\end{cases} \quad (10)$$

which is equivalent to

$$N_* = V'\left(V^{-1}(v^*)\right) = \frac{\pi}{h_{\rm go}-h_{\rm st}}\sqrt{v^*(v_{\rm max}-v^*)}\,. \quad (11)$$

Considering $\tilde{v}_{\rm L}$ as the input and $\tilde{v}$ as the output, the Laplace transform of (9) leads to the transfer function

$$\Gamma(\lambda) = \frac{\hat{K}_{\rm v}\lambda^2 + \hat{K}_{\rm p}N_*\lambda + \hat{K}_{\rm i}N_*}{\lambda^3 + \left(2\frac{k}{m}v^* + \hat{K}_{\rm p} + \hat{K}_{\rm v}\right)\lambda^2 + \left(\hat{K}_{\rm p}N_* + \hat{K}_{\rm i}\right)\lambda + \hat{K}_{\rm i}N_*}\,. \quad (12)$$

To ensure plant stability all poles (given by the denominator of the transfer function) must be on the left-half complex plane. Applying the Routh-Hurwitz criteria leads to the condition

$$\left(\hat{K}_{\rm p}N_* + \hat{K}_{\rm i}\right)\left(2\frac{k}{m}v^* + \hat{K}_{\rm p} + \hat{K}_{\rm v}\right) - \hat{K}_{\rm i}N_* > 0\,. \quad (13)$$

When crossing the plant stability boundary, there exists a pair of purely imaginary poles $\lambda = \pm{\rm i}\Omega$, so that oscillations arise with angular frequency $\Omega = \sqrt{\hat{K}_{\rm p}N_* + \hat{K}_{\rm i}}$.

To ensure string stability the inequality $|\Gamma({\rm i}\omega)| < 1$ needs to be satisfied for all $\omega \ge 0$; see [6]. Using the transfer function (12), algebraic manipulations lead to the string stability condition

$$-\omega^4 + \alpha\omega^2 + \beta < 0\,, \quad (14)$$

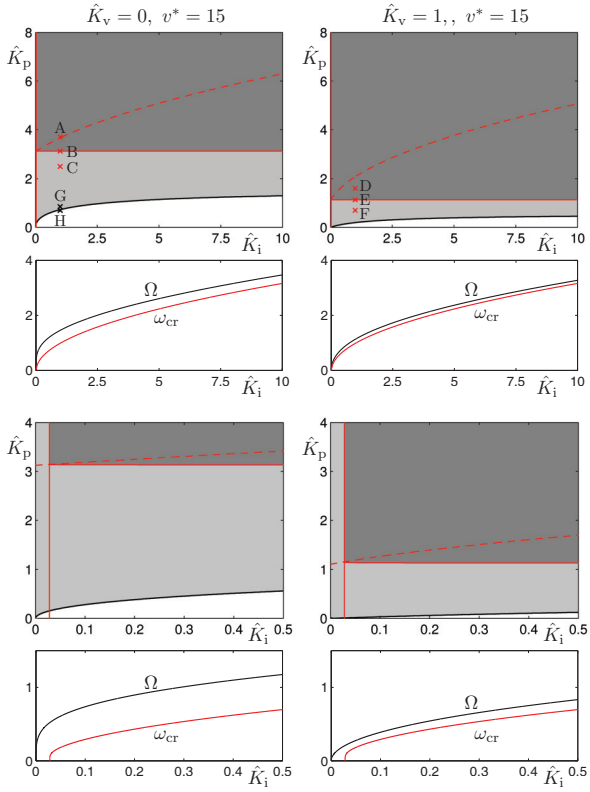

Figure 2. STABILITY DIAGRAMS IN THE $(\hat{K}_{\rm i}, \hat{K}_{\rm p})$-PLANE FOR DIFFERENT VALUES OF $\hat{K}_{\rm v}$. THE CORRESPONDING ANGULAR FREQUENCIES ARE SHOWN BELOW EACH CHART. BLACK AND RED CURVES CORRESPOND TO CHANGES IN PLANT AND STRING STABILITY, RESPECTIVELY. DARK GRAY REGIONS REPRESENT STRING STABLE PARAMETERS WHILE IN THE LIGHT GRAY REGIONS ONLY PLANT STABILITY IS ACHIEVED. ZOOMED VERSIONS OF THE UPPER PANELS ARE SHOWN IN THE LOWER PANELS.

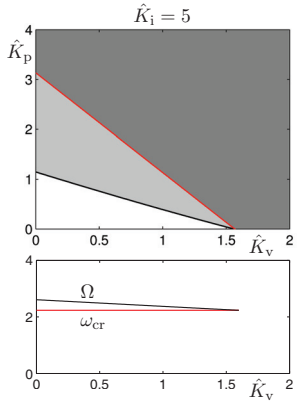

Figure 3. STABILITY DIAGRAM IN THE $(\hat{K}_{\rm v}, \hat{K}_{\rm p})$-PLANE. SAME NOTATION IS USED AS IN FIG. 2.

Copyright © 2012 by ASME

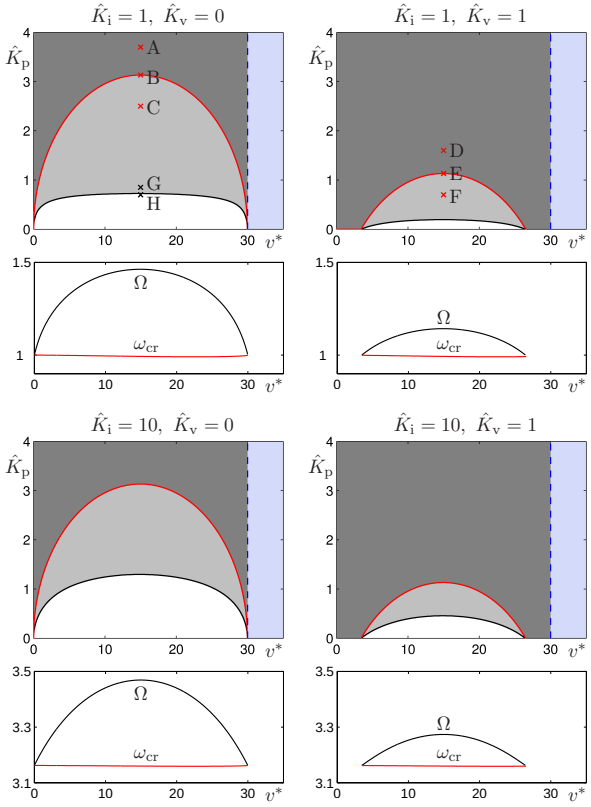

Figure 4. STABILITY CHARTS IN THE $(v^*,\hat{K}_\mathrm{p})$-PLANE FOR DIFFERENT VALUES OF $\hat{K}_\mathrm{v}$ AND $\hat{K}_\mathrm{i}$. SAME NOTATION IS USED AS IN FIG. 2.

where

$$\alpha = -\hat{K}_\mathrm{p}^2 - 2\left(2\tfrac{k}{m}v^* + \hat{K}_\mathrm{v} - N_*\right)\hat{K}_\mathrm{p} - 4\tfrac{k}{m}v^*\left(\tfrac{k}{m}v^* + \hat{K}_\mathrm{v}\right) + 2\hat{K}_\mathrm{i}\,,$$
$$\beta = \hat{K}_\mathrm{i}\left(4\tfrac{k}{m}v^*N_* - \hat{K}_\mathrm{i}\right), \qquad (15)$$

The inequality (14) is satisfied for all $\omega \geq 0$ when the following conditions hold

$$\begin{cases} \beta < 0 & \text{if} \quad \alpha \leq 0\,, \\ \alpha^2/4 + \beta < 0 & \text{if} \quad \alpha > 0\,. \end{cases} \qquad (16)$$

The condition $\beta < 0$ can be satisfied by choosing the gain

$$\hat{K}_\mathrm{i} > 4\tfrac{k}{m}v^*N_*\,. \qquad (17)$$

Using (3,10,11) one may determine that the right hand side reaches its maximum when $h^* = h_\mathrm{st} + \frac{2}{3}(h_\mathrm{go} - h_\mathrm{st})$, that is, when $v^* = \frac{3}{4}v_\mathrm{max}$, and it takes the value $\hat{K}_\mathrm{i,cr} = \frac{3}{4}\sqrt{3}\pi\frac{k}{m}v_\mathrm{max}^2/(h_\mathrm{go} - h_\mathrm{st})$. (For the parameters in Table 1 in the Appendix we have $\hat{K}_\mathrm{i,cr} \approx 0.0365$). Choosing $\hat{K}_\mathrm{i} > \hat{K}_\mathrm{i,cr}$, condition (17) is always satisfied. When $\beta < 0$ is violated the system becomes string unstable for very low frequencies. This can be explained by that the magnitude of the transfer function can be expressed as $|\Gamma(\mathrm{i}\omega)| = 1 + \omega^2\beta/(2\hat{K}_\mathrm{i}^2N_*^2) + O(\omega^4)$ for small ω. On the other hand, when $\alpha^2/4 + \beta < 0$ is violated string instability occurs in a domain of frequencies around the critical frequency $\omega_\mathrm{cr} = \sqrt{\alpha/2}$; see Fig. 5.

Fig. 2 shows the stability charts for $v^* = 15$ m/s in the $(\hat{K}_\mathrm{i},\hat{K}_\mathrm{p})$-plane for different values of $\hat{K}_\mathrm{v}$. Solid black curves represent plant stability boundaries, solid red curves represent string stability boundaries. The vertical line close to the $\hat{K}_\mathrm{i} = 0$ is the $\beta = 0$ boundary ($\beta < 0$ on the right side of the curve). The red dashed curve represents the boundary $\alpha = 0$ ($\alpha < 0$ above the curve). In the white domain the system is both string and plant unstable. Light gray shading represent parameters where the system is only plant stable, while in the dark gray regions the system is string stable (as well as plant stable). Notice that as the parameter $\hat{K}_\mathrm{v}$ is increased the stable domains grow. This can also be observed in Fig. 3 where the curves are plotted in the $(\hat{K}_\mathrm{v},\hat{K}_\mathrm{p})$-plane for a chosen value of $\hat{K}_\mathrm{i}$. Stability must be ensured in the whole velocity domain $v \in [0, v_\mathrm{max}]$. Fig. 4 shows the changes of the stability boundary in $\hat{K}_\mathrm{p}$ as a function of the equilibrium speed v^* for different values of $\hat{K}_\mathrm{i}$ and $\hat{K}_\mathrm{v}$. On may observe that larger $\hat{K}_\mathrm{p}$ is needed around the middle of the velocity domain. While the string stability boundaries only change significantly with $\hat{K}_\mathrm{v}$ the plant stability boundaries also change with $\hat{K}_\mathrm{i}$.

In Figs. 2,3 and 4 the frequencies corresponding to the plant stability (Ω) and string stability (ω_cr) are plotted below each stability chart. When crossing from the plant stable to the plant unstable domain (light gray to white) oscillations develop spontaneously with the frequency Ω. To illustrate this, we marked the points G and H on each side of the plant stability domain in Figs. 2 and 4 and plotted the corresponding time profiles in Fig. 6 (top panels) where the system is subject to constant input $v_\mathrm{L}(t) \equiv v_\mathrm{L}^*$. On the other hand, when crossing from the string stable to the string unstable domain (dark gray to light gray) oscillations close ω_cr get amplified when propagating upstream (from leader to follower). We marked the points A–F in Figs. 2 and 4 and the corresponding output-input amplitude ratios are shown in Fig. 5. Since the condition (17) is satisfied for the parameters considered here, $|\Gamma(\mathrm{i}\omega)|$ is decreasing for small frequencies in all cases. However, as the control gain $\hat{K}_\mathrm{p}$ is decreased the amplitude ratio becomes larger than 1 around the critical frequency $\omega_\mathrm{cr} \approx 1$. The smaller the $\hat{K}_\mathrm{p}$ value is the larger is the frequency domain where the system is string unstable. When comparing the diagrams for $\hat{K}_\mathrm{v} = 0$ and $\hat{K}_\mathrm{v} = 1$, observe that for the latter case the string unstable domain is smaller but the amplitude ratio increases more rapidly. The switching between string stable an string unstable behavior is illustrated by simulations in Fig. 6 (bottom panels) where the systems is subject to the periodic input $v_\mathrm{L}(t) = v_\mathrm{L}^* + v^\mathrm{amp}\sin(\omega t)$ such that the excitation frequency is close to ω_cr. While the change between the panels seems small, such small amplification/attemuation become significant as disturbances propagate along the platoon.

Copyright © 2012 by ASME

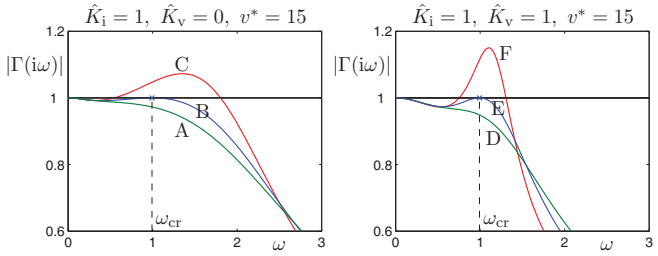

Figure 5. THE OUTPUT-INPUT AMPLITUDE RATIO IN STEADY STATE FOR SINUSODIAL INPUT FOR THE POINTS A–F MARKED IN FIGS. 2 and 4.

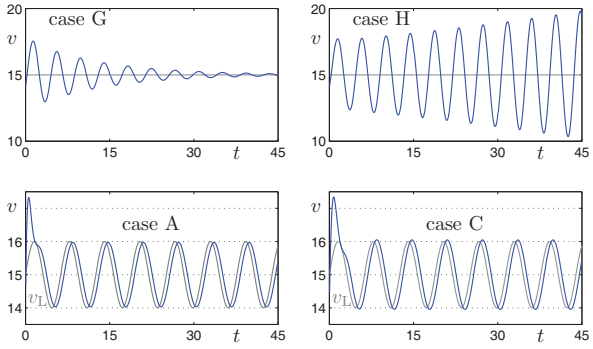

Figure 6. SIMULATION RESULTS THE POINTS A,C,D,F MARKED IN FIGS. 2 AND 4. TOP ROW: PLANT STABILITY IS TESTED BY USING THE CONSTANT INPUT $v_\mathrm{L}(t) \equiv v_\mathrm{L}^*$. BOTTOM ROW: STRING STABILITY IS TESTED USING THE OSCILLATORY INPUT $v_\mathrm{L}(t) = v_\mathrm{L}^* + v^\mathrm{amp}\sin(\omega t)$ WITH v_L^* = 15 m/s, v^amp = 1 m/s, AND ω = 1 rad/s. IN ALL CASES THE INITIAL CONDITIONS $h(0) = 22$ m, $v(0) = 14$ m/s, $z(0) = 0$ m ARE USED.

CONCLUSION AND DISCUSSION

In this paper we presented a nonlinear ACC model that allows one to operate the vehicle in both ACC mode and standard cruise control mode (and switches automatically between the two). We showed that both plant stability and string stability can be achieved by appropriately choosing the control gains and a trade-off has been found between the maximum available flux and the magnitude of the proportional gain. The obtained stability charts allow one to tune the controllers. In particular, a critical value of the integral gain $\hat{K}_\mathrm{i}$ is found that must be exceeded to maintain string stability. It is interesting to remark that string stability can be achieved without using the velocity difference between the leader and the follower (that is for $\hat{K}_\mathrm{v} = 0$) by choosing sufficiently large proportional gain $\hat{K}_\mathrm{p}$, but this may demand very large engine torque (and stall the engine). Increasing $\hat{K}_\mathrm{v}$ allows one to use more realistic $\hat{K}_\mathrm{p}$ values.

ACKNOWLEDGMENT

G.O. acknowledges the discussions with Alan Mond and Jeongyong Choi.

REFERENCES

[1] Orosz, G., Wilson, R. E., and Stépán, G., 2010. "Traffic jams: dynamics and control". *Philosophical Transactions of the Royal Society A,* **368**(1928), pp. 4455–4479.

[2] Vahidi, A., and Eskandarian, A., 2003. "Research advances in intelligent collision avoidance and adaptive cruise control". *IEEE Transactions on Intelligent Transportation Systems,* **4**(3), pp. 143–153.

[3] Ulsoy, A. G., Peng, H., and Çakmakci, M., 2012. *Automotive Control Systems*. Cambridge University Press.

[4] Kesting, A., and Treiber, M., 2008. "How reaction time, update time, and adaptation time influence the stability of traffic flow". *Computer-Aided Civil and Infrastructure Engineering,* **23**(2), pp. 125–137.

[5] Zhou, J., and Peng, H., 2005. "Range policy of adaptive cruise control vehicles for improved flow stability and string stability". *IEEE Transactions on Intelligent Transportation Systems,* **6**(2), pp. 229–237.

[6] Swaroop, D., and Hedrick, J. K., 1996. "String stability of interconnected systems". *IEEE Transactions on Automatic Control,* **41**(3), pp. 349–357.

[7] Attard, W. P., Bassett, M., Parsons, P., and Blaxill, H., 2011. "A new combustion system achieving high drive cycle fuel economy improvements in a modern vehicle powertrain". In Proceedings of the SAE 2011 World Congress & Exhibition, no. 2011-01-0664.

Appendix A: Parameters used in this paper

$m = 1555$ kg	mass of the vehicle
$C_\mathrm{d} = 0.34$	air drag coefficient
$A = 2.3$ m^2	frontal area
$\rho = 1.184$ kg/m^3	air density at 25 °C
$k = \frac{1}{2} C_\mathrm{d} \rho A = 0.463$ kg/m	
$R = 0.313$ m	tyre rolling radius
$\gamma = 0.011$	tyre rolling resistance coefficient
$g = 9.81$ m/s^2	gravitational constant
$\ell = 5$ m	vehicle length (approximation)
$v_\mathrm{max} = 30$ m/s	desired maximum velocity
$h_\mathrm{st} = 5$ m	desired stopping distance
$h_\mathrm{go} = 35$ m	minimal free flow distance

Table 1. Data of a 2011 Chevrolet HHR vehicle [7] are shown together with the parameters used for the range policy.

Copyright © 2012 by ASME